

DSPFusion: Image Fusion via Degradation and Semantic Dual-Prior Guidance

Linfeng Tang¹ Chunyu Li¹ Guoqing Wang² Yixuan Yuan³ Jiayi Ma^{1*}
¹Wuhan University ²University of Electronic Science and Technology of China
³The Chinese University of Hong Kong

linfeng0419@gmail.com licy0089@gmail.com gqwang0420@hotmail.com
yxyuan@ee.cuhk.edu.hk jyama2010@gmail.com

Abstract

*Existing fusion methods are tailored for high-quality images but struggle with degraded images captured under harsh circumstances, thus limiting the practical potential of image fusion. This work presents a **Degradation and Semantic Prior dual-guided framework for degraded image Fusion (DSPFusion)**, utilizing degradation priors and high-quality scene semantic priors restored via diffusion models to guide both information recovery and fusion in a unified model. In specific, it first individually extracts modality-specific degradation priors, while jointly capturing comprehensive low-quality semantic priors. Subsequently, a diffusion model is developed to iteratively restore high-quality semantic priors in a compact latent space, enabling our method to be over 20× faster than mainstream diffusion model-based image fusion schemes. Finally, the degradation priors and high-quality semantic priors are employed to guide information enhancement and aggregation via the dual-prior guidance and prior-guided fusion modules. Extensive experiments demonstrate that DSPFusion mitigates most typical degradations while integrating complementary context with minimal computational cost, greatly broadening the application scope of image fusion.*

1. Introduction

Image fusion is a fundamental enhancement technique designed to combine complementary context from multiple images, thereby overcoming limitations of single-modality or single-type sensors [49]. Infrared-visible image fusion (IVIF) is a key research area in image fusion, integrating essential thermal information from infrared (IR) images with the rich textures of visible (VI) images for comprehensive scene characterization [53]. The complete information integration and visually pleasing results make IVIF widely ap-

plied in military detection [23], security surveillance [54], assisted driving [1], scene understanding [8, 52], etc.

Recently, IVIF has garnered significant attention, leading to rapid advancements in relevant algorithms, which can be classified into convolutional neural network- [21, 55], autoencoder- [12, 13], generative adversarial network- [16, 20], Transformer- [22, 51], and diffusion model (DM)-based [43, 57] methods. Moreover, from a functional perspective, they can be categorized into visual-oriented [20, 33], degradation-aware [34, 50], semantic-driven [17, 32], and joint registration-fusion [31, 42] schemes. Despite the satisfactory fusion performance achieved by these methods, several challenges still remain. On the one hand, while DMs with powerful generative abilities could bring gains, DM-based fusion methods [47, 57] are often computationally intensive and time-consuming, making them inapplicable in real-time tasks. On the other hand, although some degradation-aware methods have been proposed to address imaging interferences, they still struggle with complex fusion scenarios. For example, DIVFusion [34] and PAIF [18] are tailored for specific degradations (e.g., low-light or noise) yet fail to generalize to others. Additionally, some general degradation-aware methods handle multiple degradations within a single framework assisted by additional semantic context, such as text prompts [44]. However, they are sensitive to text prompts and struggle to handle cases where degradations occur simultaneously in both infrared and visible images. Moreover, tailoring text descriptions for each fusion scenario is challenging.

To overcome the above challenges, we propose a degradation and semantic prior dual-guided image fusion framework, abbreviated as DSPFusion, which incorporates degradation suppression and information aggregation in a unified model without additional assistance. The proposed method involves two training phases. In Stage I, the semantic prior embedding network (SPEN) captures the semantic prior from cascaded high-quality sources, while the degradation prior embedding network (DPEN) extracts distinct degradation priors from two degraded images sepa-

*Corresponding author.

rately. A Transformer-based restoration and fusion network, guided by degradation and semantic priors, synthesizes high-quality fusion results. Note that the scene semantic prior is jointly derived from both modalities, enabling our model to enhance one using high-quality context from its complementary modality. We employ a contrastive mechanism to train DPEN, thus ensuring degradation priors effectively characterize various degradation types. Since high-quality source images are unavailable in practical situations, we deploy a diffusion model to restore high-quality semantic priors from low-quality ones in Stage II. The diffusion process is performed in a compact latent space, making our model computationally efficient and lightweight. Ultimately, DPEN adaptively identifies degradation types and a diffusion model refines semantic priors, aiding the restoration and fusion model in synthesizing high-quality fusion results. In summary, our main contributions are as follows:

- We propose a novel restoration and fusion framework with dual guidance of degradation and semantic priors, effectively handling most typical degradations (*e.g.*, low-light, over-exposure, noise, blur, and low-contrast) while aggregating complementary information from multiple modalities in a unified model. To our knowledge, it is the first model that comprehensively addresses various degradations in image fusion.
- A diffusion model is devised to restore high-quality semantic priors in a compact latent space, providing coarse-grained semantic guidance with low computational cost.
- A contrastive mechanism is employed to constrain DPEN to adaptively perceive degradation types, thereby guiding the restoration and fusion network as well as the semantic prior diffusion model to purposefully handle degradations without requiring additional auxiliary information.
- Extensive experiments on normal and degraded scenarios demonstrate the superiority of our method in degradation suppression and complementary context aggregation.

2. Related Work

Image Fusion. Earlier visual-oriented fusion methods focus on integrating cross-modal complementary context and enhancing visual quality, which rely on elaborate network architectures and loss functions to preserve complementary information that remains faithful to source images. Initially, mainstream network architectures primarily include CNN [15, 55], AE [13, 56], and GAN [16, 20]. With the rise of Transformers [36] and diffusion models [7], these architectures gradually dominate fusion model design [22, 47]. However, as a compute-intensive process, the time cost of diffusion models remains a contentious issue.

Furthermore, several schemes including joint registration and fusion [37, 41, 42], semantic-driven [16, 30, 32], and degradation-aware [18, 34] methods, are proposed to broaden the practical applications of image fusion. Par-

ticularly, under some extreme conditions, environmental factors like low light and noise inevitably affect imaging. Thus, Tang et al. [34] proposed an illumination-robust fusion method, achieving low-light enhancement and complementary context aggregation simultaneously. Liu et al. [18] developed a perception-aware method by leveraging adversarial attack and architecture search to boost the robustness against noise. However, these methods are tailored to specific degradations and struggle with complex and diverse interferences. To this end, Yi et al. [44] leveraged CLIP to extract semantic embedding from texts to assist the fusion network in addressing multiple degradations. However, customizing text for each scenario is costly and impractical. Therefore, it is urgent and challenging to directly identify degradation types from source images, allowing a unified network to effectively handle diverse degradations and achieve optimal information aggregation.

Unified Image Restoration. With advancements in deep learning technology, the field of image restoration is evolving beyond designing specialized models for specific degradation factors. Initially, researchers modeled different degradations uniformly and trained task-specific headers [2] or separate models [39, 48] to address various degradations. Furthermore, PromptIR [25] and AutoDIR [10] interpret textual user requirements via the CLIP encoder [26], guiding the general restoration models to deal with diverse degradations. To avoid reliance on user input, [11] employed contrastive learning to identify degradation types from corrupted images and guide restoration models in addressing corruptions via feature modulation. Similarly, [19] fine-tuned CLIP on their mixed degradation dataset to develop DA-CLIP, which directly perceives degradation types and predicts high-quality content embeddings from corrupted inputs, aiding restoration networks in handling various degradations. Note that these unified restoration models are designed for natural images and usually not applicable to multi-modal images, such as infrared and visible images.

Diffusion Model. Benefiting from their powerful generative capabilities, diffusion models (DMs) have been applied to diverse applications such as text-to-image generation [28], image restoration [39], super-resolution [29], deblurring [4], and deraining [24], consistently delivering impressive results. DMs have also been applied to the image fusion task. Yue et al. [47] utilized the denoising network of DMs to enhance feature extraction. Zhao et al. [57] integrated a pre-trained DM into the EM algorithm, achieving multi-modal fusion with generative priors from natural images. However, these schemes perform the diffusion process in the image domain, making DM-based methods time-consuming. To improve efficiency, some approaches, such as Stable Diffusion [28], PVDM [46], and Hi-Diff [4], transfer the diffusion process into a latent space.

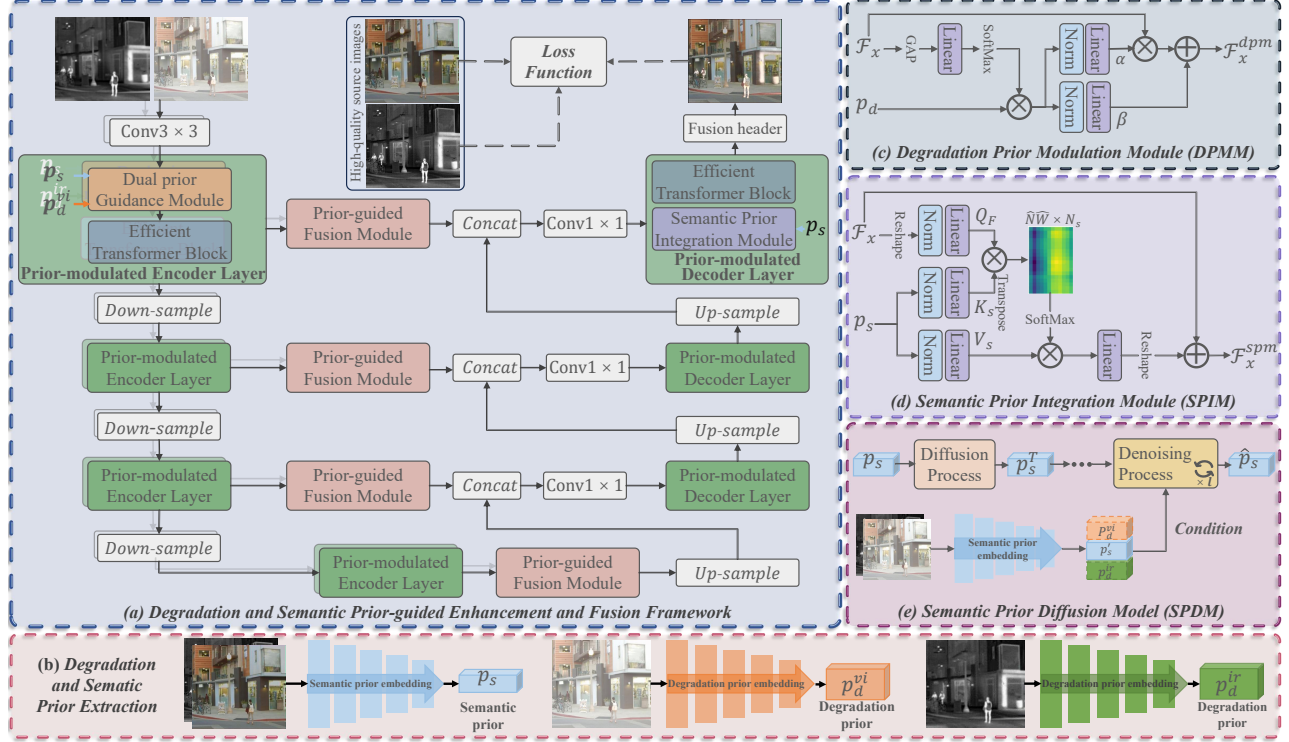


Figure 1. The overall framework of our image fusion network with degradation and semantic dual-prior guidance.

3. Methodology

3.1. Overview

Our workflow is illustrated in Fig. 1. Given low-quality visible image I_{vi}^{lq} and infrared image I_{ir}^{lq} , we first extract global low-quality semantic prior (\hat{p}_s) and degradation priors (p_d^{vi} and p_d^{ir}) via the semantic prior embedding network (SPEN, \mathcal{N}_s) and degradation prior embedding network (DPEN, \mathcal{N}_d), described as:

$$\begin{aligned} \hat{p}_s &= \mathcal{N}_s(I_{vi}^{lq}, I_{ir}^{lq}; \theta_s), \\ \{p_d^{vi}, p_d^{ir}\} &= \{\mathcal{N}_d(I_{vi}^{lq}; \theta_d), \mathcal{N}_d(I_{ir}^{lq}; \theta_d)\}, \end{aligned} \quad (1)$$

where θ denotes the network parameter. Then, a semantic prior diffusion model (SPDM, \mathcal{N}_{dm}) is designed to restore high-quality semantic prior (p'_s) from \hat{p}_s guided by degradation priors, which is formulated as:

$$p'_s = \mathcal{N}_{dm}(\hat{p}_s, p_d^{vi}, p_d^{ir}; \theta_{dm}). \quad (2)$$

Finally, p'_s , p_d^{vi} , and p_d^{ir} are employed together to assist the restoration and fusion network (\mathcal{N}_{ef}) in synthesizing high-quality fused images (I_f):

$$I_f = \mathcal{N}_{ef}(I_{vi}^{lq}, I_{ir}^{lq}, p_d^{vi}, p_d^{ir}, p'_s; \theta_{ef}). \quad (3)$$

\mathcal{N}_{ef} is a successor of Restormer [48]. Specifically, we develop two parallel branches to extract multi-scale vis-

ible and infrared features, while integrating the degradation and semantic priors to counteract various degradations. The k -th level feature extraction is defined as $\mathcal{F}_x^k = E_k(\mathcal{F}_x^{k-1}, p_d^x, p_s)$, where $x \in \{ir, vi\}$, E_k denotes the k -th level prior-modulated encoder layer. Then, the semantic prior-guided fusion module (PGFM, \mathcal{M}_f) is employed to aggregate the complementary information on each level and output F_f , formulated as $\mathcal{F}_f^k = \mathcal{M}_f(\mathcal{F}_{ir}^k, \mathcal{F}_{vi}^k, p_s)$. The prior-modulated decoder layers then refine fused features from coarse to fine-grained. Finally, a fusion header generates high-quality fusion results (I_f). Following previous practice [4, 39], we train our DSPFusion with a two-stage training strategy, where Stage I focuses on prior extraction and modulation, and Stage II optimizes the SPDM.

3.2. Stage I: Prior Extraction and Modulation

Stage I aims to compress high- and low-quality images into a compact latent space to characterize scene semantics and degradation types, thus guiding restoration and fusion.

3.2.1. Network Architectures

Degradation and Semantic Embedding. As shown in Fig. 1 (b), high-quality images I_{vi}^{hq} and I_{ir}^{hq} are jointly fed into the semantic prior embedding network (SPEN) to obtain a compact semantic prior p_s . In parallel, I_{vi}^{lq} and I_{ir}^{lq} are processed separately by the degradation prior embedding network (DPEN) to capture degradation priors p_d^{vi} and

p_d^{ir} . SPEN and DPEN share a similar structure with residual blocks to generate prior embeddings $p \in \mathbb{R}^{N \times C'}$, where N and C' represent the token number and channel dimension. Notably, N is much smaller than $H \times W$, resulting in a higher compression ratio ($\frac{H \times W}{N_s}$) compared to previous latent diffusion models (e.g., 8) [28], significantly reducing the computational burden of subsequent SPDM. Additionally, the distribution of the latent semantic space ($\mathbb{R}^{N \times C'}$) is simpler than that of the image space ($\mathbb{R}^{H \times W \times 3}$), which can be approximated with fewer iterations. Thus, SPDM only requires fewer sampling steps ($T \ll 1000$) to infer semantic priors compared to mainstream image-level DM-based fusion schemes [57], further decreasing computational cost.

Dual Prior Guidance Module. We integrate these priors into \mathcal{N}_{ef} via the dual prior guidance module (DPGM). In particular, input features \mathcal{F}_x first pass through the parallel degradation prior modulation module (DPMM) and semantic prior integration module (SPIM). As shown in Fig. 1 (c), \mathcal{F}_x is compressed into a vector matching the size of p_d^x and then multiplied by p_d^x . The resulting product passes through a linear layer to output the modulation parameters α_d^x and β_d^x . Then, DPMM is formulated as $\mathcal{F}_x^{dpm} = (\alpha_d^x \otimes \mathcal{F}_x) \oplus \beta_d^x$, referring to [11, 44]. In parallel, the semantic prior is integrated into \mathcal{F}_x through SPIM to enhance its global perception of high-quality scene context. As shown in Fig. 1 (d), \mathcal{F}_x is mapped as a query $Q_F \in \mathbb{R}^{\hat{H}\hat{W} \times C'}$, and p_s is mapped as the key $K_s \in \mathbb{R}^{N_s \times C'}$ and value $V_s \in \mathbb{R}^{N_s \times C'}$. Then, cross-attention is applied to perform semantic prior integration and generate the semantic-modulated features as:

$$\mathcal{F}_x^{spi} = \mathcal{F}_x \oplus \text{softmax} \left(Q_F K_s^T / \sqrt{d_k} \right) V_s, \quad (4)$$

where d_k is a learnable scaling factor. Then, we also employ the cross-attention mechanism to aggregate \mathcal{F}_x^{dpm} and \mathcal{F}_x^{spi} to obtain final reinforcement features with $\mathcal{F}_x^{dpg} = \mathcal{F}_x^{spi} \oplus \text{softmax} \left(Q_{spi} K_{dpm}^T / \sqrt{d_k} \right) V_{dpm}$, where Q_{spi} is mapped from \mathcal{F}_x^{spi} , and K_{dpm} and V_{dpm} are mapped from \mathcal{F}_x^{dpm} . Importantly, p_s provides global semantic guidance, and p_d explicitly indicates degradation types, thereby reducing the overall training difficulty of restoration.

Prior-Guided Fusion Module. Considering that p_s is jointly extracted from multi-modal inputs, implicitly achieving complementary context aggregation, we utilize it to generate channel-wise fusion weights. Moreover, a spatial attention mechanism is utilized to calculate spatial-wise weights that, along with channel-wise weights, yield the final fusion weights w_{ir}^k and w_{vi}^k . Finally, complementary feature fusion is formulated as: $\mathcal{F}_f^k = w_{ir}^k \mathcal{F}_{ir}^k \oplus w_{vi}^k \mathcal{F}_{vi}^k$.

Image Reconstruction. The multi-scale fused features are refined from coarse to fine using prior-modulated decoder layers, which utilize the SPIM rather than the DPGM, relying exclusively on high-quality scene semantic priors to enhance feature reinforcement. Subsequently, a fusion

header, structurally similar to the decoder layer, generates I_f from enhanced fused features (\mathcal{F}_f^0). More network details can be found in the **Supple. Material**.

3.2.2. Loss Functions

Since degradation and semantic priors are abstract high-dimensional features without ground-truth constraints, we use fusion and contrastive losses to jointly optimize \mathcal{N}_{ef} , \mathcal{N}_s , and \mathcal{N}_d . Following Ma et al. [22] and Yi et al. [44], the fusion loss involves content, structural similarity (SSIM), and color consistency losses. To counteract degradations, we construct these losses with manually obtained high-quality source images. The content loss is defined as:

$$\mathcal{L}_{cont} = \frac{1}{HW} (\|I_f - \max(I_{vi}^{hq}, I_{ir}^{hq})\|_1 + \gamma \cdot \|\nabla I_f - \max(\nabla I_{vi}^{hq}, \nabla I_{ir}^{hq})\|_1), \quad (5)$$

where ∇ means the Sobel operator, $\max(\cdot)$ is the maximum selection for preserving salient targets and textures, $\|\cdot\|_1$ and γ are the l_1 -norm and trade-off parameter. The SSIM loss is applied to maintain the structural similarity between the fused image and high-quality sources, formulated as:

$$\mathcal{L}_{ssim} = (1 - \text{SSIM}(I_f, I_{vi}^{hq})) + (1 - \text{SSIM}(I_f, I_{ir}^{hq})). \quad (6)$$

Moreover, we construct the color consistency loss to encourage fused images to preserve color information from high-quality visible images. It is defined as:

$$\mathcal{L}_{color} = \frac{1}{HW} \|\Phi_{CbCr}(I_f) - \Phi_{CbCr}(I_{vi}^{hq})\|_1, \quad (7)$$

where $\Phi_{CbCr}(\cdot)$ converts RGB to CbCr. Besides, our DPEN aims to adaptively identify various degradations. For inputs with different degradations, the corresponding p_d should be distinct, even if image contents are the same. To achieve this, we devise a contrastive loss \mathcal{L}_{cl} that pulls together priors characterizing same degradations while pushing apart priors representing various degradations. For a degradation prior p_d , q_k^+ and q_m^- are the corresponding positive and negative counterparts. Then, \mathcal{L}_{cl} is formulated as:

$$\mathcal{L}_{cl} = \sum_{k=1}^K -\log \frac{\exp(p_d \cdot q_k^+ / \tau)}{\sum_{m=1}^M \exp(p_d \cdot q_m^- / \tau)}, \quad (8)$$

where K and M are the number of positive and negative samples, and τ is a temperature parameter. If p_d is extracted from an image with a specific degradation, then q_k^+ is extracted from other scenes with the same degradation, while q_m^- is extracted from the same scene but with various degradations or modalities. Finally, the total loss of Stage I is formulated as the weighted sum of aforementioned losses:

$$\mathcal{L}_I = \lambda_{cont} \cdot \mathcal{L}_{cont} + \lambda_{ssim} \cdot \mathcal{L}_{ssim} + \lambda_{color} \cdot \mathcal{L}_{color} + \lambda_{cl} \cdot \mathcal{L}_{cl}, \quad (9)$$

where λ_{cont} , λ_{ssim} , λ_{color} , and λ_{cl} are hyper-parameters.

Table 1. Quantitative comparison results on typical fusion datasets. The best and second-best results are highlighted in Red and Purple.

Methods	MSRS				LLVIP				RoadScene				TNO			
	EN	MI	VIF	Qabf	EN	MI	VIF	Qabf	EN	MI	VIF	Qabf	EN	MI	VIF	Qabf
DeFus. [15]	6.350	3.054	0.736	0.505	7.112	3.196	0.683	0.487	6.910	3.018	0.537	0.404	6.581	2.917	0.596	0.384
PAIF [18]	5.830	2.907	0.470	0.329	6.937	2.533	0.432	0.286	6.750	2.919	0.387	0.248	6.198	2.561	0.421	0.243
MetaFus. [55]	6.355	1.693	0.700	0.476	6.645	1.400	0.629	0.429	7.363	2.195	0.517	0.416	7.184	1.815	0.615	0.362
LRNet [13]	6.197	2.886	0.536	0.451	6.006	1.749	0.397	0.281	7.051	2.649	0.463	0.344	6.944	2.577	0.577	0.352
MURF [42]	5.036	1.516	0.403	0.311	5.869	2.017	0.355	0.317	6.961	2.492	0.498	0.468	6.654	1.912	0.528	0.378
SegMiF [17]	6.109	2.472	0.774	0.565	7.172	2.819	0.837	0.651	7.254	2.657	0.615	0.543	6.976	3.036	0.876	0.589
DDFM [57]	6.182	2.661	0.721	0.468	6.814	2.590	0.632	0.475	7.111	2.84	0.587	0.482	6.878	2.408	0.691	0.466
EMMA [58]	6.713	4.129	0.957	0.632	7.160	3.374	0.740	0.572	7.383	3.140	0.605	0.461	7.203	3.038	0.755	0.472
Text-IF [44]	6.648	4.283	1.031	0.692	6.961	3.142	0.855	0.648	7.299	2.988	0.698	0.588	7.168	3.524	0.918	0.583
DSPFusion	6.695	4.736	1.044	0.726	7.314	4.390	0.943	0.717	7.363	3.962	0.755	0.667	7.152	4.680	0.931	0.640

3.3. Stage II: Semantic Prior Diffusion Model

In Stage II, we develop a semantic prior diffusion model (SPDM) to restore high-quality semantic prior from low-quality ones, thereby guiding restoration and fusion. SPDM involves the forward diffusion and reverse denoising processes, as shown in Fig. 1 (e). In the diffusion process, we first embed I_{vi}^{hq} and I_{ir}^{hq} into a high-quality semantic prior p_s , which is simply marked as x_0 in this section. x_0 serves as the starting point of a forward Markov chain and gradually adds Gaussian noise to it over T iterations as:

$$\begin{aligned} q(x_{1:T}|x_0) &= \prod_{t=1}^T q(x_t|x_{t-1}), \\ q(x_t|x_{t-1}) &= \mathcal{N}(x_t; \sqrt{\alpha_t}x_{t-1}, \beta_t\mathbf{I}), \end{aligned} \quad (10)$$

where x_t is the t -step noisy variable, β_t governs noise variance, and $\alpha_t = 1 - \beta_t$. Through iterative derivation with reparameterization, the forward process is reformulated as:

$$q(x_t|x_0) = \mathcal{N}(x_t, \sqrt{\bar{\alpha}_t}x_0, (1 - \bar{\alpha}_t)\mathbf{I}), \quad (11)$$

where $\bar{\alpha}_t = \prod_{i=1}^t \alpha_i$. As t approaches a large value T , $\bar{\alpha}_T$ tends to 0 and $q(x_T|x_0)$ approximates the normal distribution $\mathcal{N}(0, \mathbf{I})$, thus completing the forward process.

The reverse process starts from a pure Gaussian distribution and progressively denoises to generate the high-quality semantic prior via a T -step Markov chain, defined as:

$$p(x_{t-1}|x_t) = \mathcal{N}(x_{t-1}; \mu(x_t, t), \sigma_t^2\mathbf{I}), \quad (12)$$

with $\mu(x_t, t) = \frac{1}{\sqrt{\alpha_t}}(x_t - \frac{\beta_t}{\sqrt{1-\alpha_t}}\epsilon)$, and $\sigma_t^2 = \frac{(1-\bar{\alpha}_{t-1})}{(1-\bar{\alpha}_t)}\beta_t$. Following previous works [7, 28], we employ a denoising U-Net (ϵ_θ) with the aid of the low-quality semantic prior \hat{p}_s and degradation priors p_d^{vi} and p_d^{ir} to estimate the noise ϵ . Utilizing the reparameterization trick and substituting ϵ in Eq. (12) with $\epsilon_\theta(x_t, \hat{p}_s, p_d^{vi}, p_d^{ir}, t)$, we can get:

$$x_{t-1} = \frac{1}{\sqrt{\alpha_t}} \left(x_t - \frac{1 - \alpha_t}{\sqrt{1 - \bar{\alpha}_t}} \epsilon_\theta(x_t, \hat{p}_s, p_d^{vi}, p_d^{ir}, t) \right) + \sigma_t z. \quad (13)$$

Traditionally, the objective for training ϵ_θ is defined as:

$$\nabla_\theta \|\epsilon_t - \epsilon_\theta(\sqrt{\alpha_t}x_0 + \sqrt{1 - \bar{\alpha}_t}\epsilon_t, \hat{p}_s, p_d^{vi}, p_d^{ir}, t)\|_2^2. \quad (14)$$

Since the distribution of the latent semantic space ($\mathbb{R}^{N_s \times C'}$) is simpler than that of the image space ($\mathbb{R}^{H \times W \times 3}$), the semantic prior (p'_s) can be generated with fewer iterations [4]. Thus, we run complete T ($\ll 1000$) reverse iterations to infer p'_s . Consequently, we use $\mathcal{L}_{diff} = \|p'_s - p_s\|_1$ to train SPDM. We also apply the content, SSIM, and color consistency losses to collaboratively constrain the training of SPDM. Thus, the total loss of Stage II is defined as:

$$\mathcal{L}_{II} = \lambda_d \cdot \mathcal{L}_{diff} + \lambda_{cont} \cdot \mathcal{L}_{cont} + \lambda_{ssim} \cdot \mathcal{L}_{ssim} + \lambda_{color} \cdot \mathcal{L}_{color}, \quad (15)$$

where λ_d is a hyper-parameter for balancing various losses.

4. Experiments

4.1. Experimental Details

Implementation Details. Our restoration and fusion network inherits Restormer [48], a 4-level encoder-decoder Transformer architecture with degradation and semantic prior modulation. From level-1 to level-4, Transformer block numbers are set as [2, 2, 4, 4], and channel numbers are set as [32, 64, 128, 256]. SPEN contains 6 residual blocks with token number and channel dimension set to $N_c = 16$ and $C'_c = 256$. DPEN contains 4 residual blocks with token number and channel dimension set to $N_d = 16$ and $C'_d = 128$. The time-step of SPDM is set as $T = 10$. We train our DSPFusion with the AdamW optimizer with $\beta_1 = 0.9$ and $\beta_2 = 0.99$. The learning rate is initialized to 2×10^{-4} and gradually reduced to 1×10^{-6} with cosine annealing. Both Stages I and II are trained for $50k$ iterations. The hyper-parameters are empirically set as $\gamma = 0.75$, $\lambda_{cont} = 15$, $\lambda_{ssim} = 2$, $\lambda_{color} = 20$, $\lambda_{cl} = 1$, $\lambda_d = 10$. The numbers of positive and negative samples are set to $K = 3$ and $M = 7$. Our training data is construed on the EMS dataset [44], including 2, 210 scenarios, with 8, 804 and 10, 318 low-quality infrared and visible images.

Table 2. Quantitative comparison results in different degraded scenarios with pre-enhancement.

Methods	VI (Blur)				VI (Rain)				VI (Low-light, LL)				VI (Over-exposure, OE)			
	MUSIQ	PI	TReS	SF	MUSIQ	PI	TReS	SD	MUSIQ	PI	TReS	SD	MUSIQ	PI	TReS	SD
DeFus. [15]	38.971	4.368	36.968	8.765	44.182	3.575	44.516	40.471	43.645	3.510	42.961	36.326	46.316	3.367	45.972	38.649
PAIF [18]	39.363	5.431	40.298	9.102	45.685	4.720	46.819	38.593	42.432	4.725	45.248	39.239	37.032	5.261	35.094	52.062
MetaFus. [55]	36.674	4.946	34.451	18.167	41.160	4.127	39.105	49.808	38.775	4.061	33.915	46.852	43.590	3.217	38.889	52.473
LRRNet [13]	41.490	4.074	41.774	11.084	48.591	3.218	50.646	42.612	44.037	3.391	47.584	31.204	48.263	2.803	51.459	44.852
MURF [42]	45.860	3.379	46.603	12.374	48.703	3.131	49.965	25.117	44.979	3.144	46.383	21.418	52.484	2.518	56.603	33.128
SegMiF [17]	42.907	4.02	41.349	12.636	47.850	2.909	50.016	46.861	45.16	3.049	46.311	45.614	51.282	2.688	54.419	50.445
DDFM [57]	42.005	3.928	42.765	9.474	47.117	3.229	49.757	36.140	44.022	3.346	47.090	32.197	52.182	2.435	59.047	41.834
EMMA [58]	41.442	4.128	37.81	14.036	48.315	3.078	45.750	55.989	45.124	3.201	42.383	45.881	49.446	2.651	48.389	54.538
Text-IF [44]	44.536	3.665	47.524	15.153	50.109	2.775	56.966	54.842	46.015	2.994	50.279	51.537	52.048	2.290	56.979	52.200
DSPFusion	47.137	2.972	49.750	15.693	50.467	2.557	56.528	55.599	48.500	2.768	54.090	45.940	52.812	2.206	57.198	54.840
Methods	VI (Random noise, RN)				IR (Low-contrast, LC)				IR (Random noise, RN)				IR (Stripe noise, SN)			
	MUSIQ	PI	TReS	EN	MUSIQ	PI	TReS	SD	MUSIQ	PI	TReS	EN	MUSIQ	PI	TReS	EN
DeFus. [15]	34.661	4.883	30.837	7.028	44.378	3.538	45.154	39.753	40.463	3.735	43.565	7.065	42.603	3.593	42.966	6.968
PAIF [18]	33.875	6.306	33.362	6.731	47.192	4.525	47.946	38.499	47.198	4.456	49.016	6.772	47.403	4.482	48.921	6.747
MetaFus. [55]	32.918	4.969	27.623	7.362	40.136	4.224	39.847	55.705	40.236	4.304	39.461	7.419	39.543	4.215	38.837	7.448
LRRNet [13]	34.856	4.642	32.07	7.108	48.540	3.189	50.456	42.697	46.625	3.327	49.883	7.015	47.382	3.248	48.708	7.016
MURF [42]	40.866	3.386	42.447	6.233	48.958	3.063	51.079	26.875	49.799	3.276	49.431	6.204	47.135	3.202	47.908	6.223
SegMiF [17]	37.362	4.081	31.640	6.975	48.335	2.803	51.976	50.813	47.909	2.977	50.489	6.997	46.971	2.852	49.394	7.080
DDFM [57]	37.325	4.351	36.870	6.940	48.039	3.222	51.181	37.090	46.829	3.512	48.653	6.960	45.310	3.361	47.234	6.908
EMMA [58]	34.754	4.432	29.364	7.44	48.721	2.978	46.842	58.299	45.870	3.124	45.667	7.453	47.286	3.036	45.717	7.439
Text-IF [44]	39.200	3.930	36.588	7.406	50.022	2.794	55.203	56.117	48.795	2.944	54.003	7.402	49.376	2.829	53.717	7.440
DSPFusion	47.718	2.954	52.787	7.343	50.597	2.623	56.988	56.060	50.752	2.852	57.266	7.349	51.055	2.787	57.243	7.353
Methods	VI (Rain) and IR (LC)				VI (Rain) and IR (SN)				VI (LL) and IR (LC)				VI (LL) and IR (SN)			
	MUSIQ	PI	TReS	SD	MUSIQ	PI	TReS	EN	MUSIQ	PI	TReS	SD	MUSIQ	PI	TReS	EN
DeFus. [15]	44.168	3.727	44.601	35.803	41.933	3.808	42.020	6.827	42.000	3.654	41.607	30.416	40.279	3.684	38.722	6.788
PAIF [18]	46.172	4.817	46.361	37.658	46.013	4.778	47.135	6.661	42.671	4.639	46.503	30.425	41.686	4.796	44.084	6.616
MetaFus. [55]	40.528	4.221	39.237	51.363	40.175	4.214	38.272	7.339	38.832	3.833	33.506	43.002	37.957	4.086	31.719	7.194
LRRNet [13]	48.396	3.248	50.05	42.434	47.151	3.335	48.290	6.999	43.231	3.414	45.943	31.170	42.730	3.564	44.534	6.630
MURF [42]	49.221	3.082	50.669	26.013	47.048	3.271	47.253	6.148	44.943	3.117	45.792	18.915	43.006	3.300	42.568	5.910
SegMiF [17]	48.392	2.915	50.802	46.525	46.548	2.998	47.923	6.989	44.512	2.965	45.744	40.511	43.337	3.218	43.201	6.982
DDFM [57]	47.513	3.318	50.074	36.381	44.869	3.447	46.338	6.873	43.242	3.473	46.691	29.616	41.600	3.788	43.711	6.722
EMMA [58]	48.864	3.017	46.307	54.659	47.216	3.119	45.023	7.366	44.251	3.211	41.010	43.038	43.652	3.233	39.788	7.209
Text-IF [44]	50.380	2.765	56.429	56.381	48.221	2.885	53.446	7.400	47.815	2.915	49.334	45.733	39.866	3.272	39.043	7.095
DSPFusion	50.672	2.607	56.362	55.686	50.883	2.737	57.098	7.349	48.547	2.819	53.892	46.144	48.711	3.020	54.598	7.263

Experiment Settings. We first compare DSPFusion with nine SOTA fusion methods on four typical datasets (MSRS [33], LLVIP [9], RoadScene [40], TNO [35]) with 4 quantitative metrics, *i.e.*, EN, MI, VIF, and Q_{abf} . Then, we validate its performance under various degradations, including blur, rain, low-light, over-exposure, and random noise in visible (VI), and low-contrast, random noise, and stripe noise in infrared (IR). We also evaluate our robustness under mixed degradations, *i.e.*, rain or low-light in VI, and low-contrast or stripe noise in IR. All scenarios include 100 test samples, except for over-exposure in VI, containing 50 test samples. Four no-reference metrics, *i.e.*, MUSIQ, PI, TReS, and SD (or EN or SF), are used to verify fusion qualities. SOTA restoration algorithms are deployed to pre-enhance low-quality sources if fusion methods without enhancement for fair comparisons. Particularly, Hi-Diff [4] for deblurring, NeRD-Rain [3] for deraining, Spadap [14] for denoising, QuadPrior [38] for low-light enhancement, IAT [5] for exposure correction, WDN [6] for stripe noise removal, and the method in [33] for low-contrast enhancement.

4.2. Fusion Performance Comparison

Comparison without Pre-Enhancement. Table 1 shows quantitative results on typical fusion datasets. DSPFusion achieves superior performance in MI and Q_{abf} , effectively transferring complementary and edge information into fused images. The optimal VIF indicates that our fused images exhibit excellent visual perception quality, while the comparable EN suggests that our fusion results retain abundant information. In summary, the quantitative results demonstrate our remarkable fusion performance. Some visual fusion results are provided in the **Supple. Material**.

Comparison with Pre-Enhancement. The quantitative results in degraded scenarios are shown in Tab. 2. DSPFusion achieves the best MUSIQ, PI, and TReS in almost all degraded scenarios, demonstrating its effectiveness in mitigating degradation, aggregating complementary context, and producing high-quality fused images. We apply various no-reference statistical metrics, *i.e.*, SD, EN, or SF, to evaluate fusion results on different degraded scenarios ac-

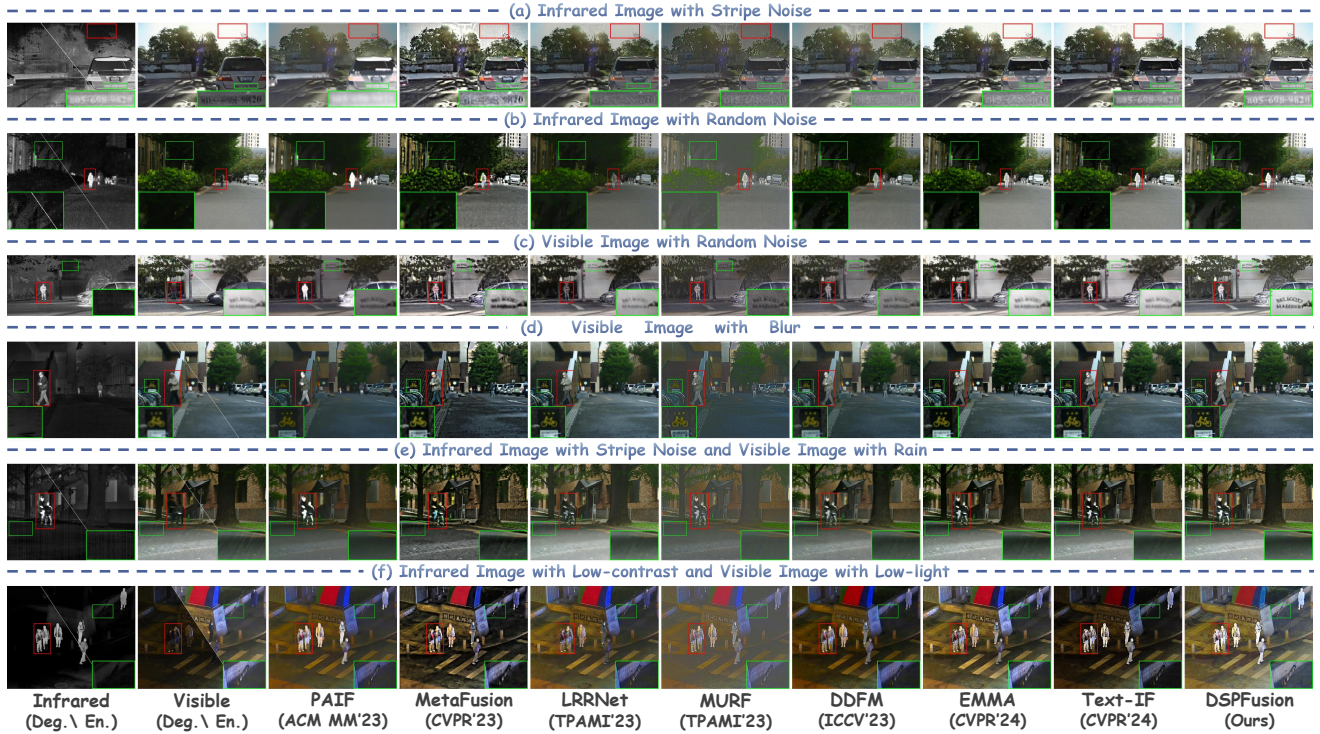


Figure 2. Visualization of fusion results in different degraded scenarios with pre-enhancement.

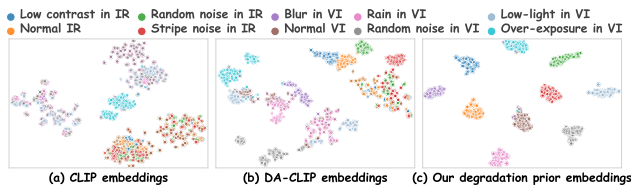


Figure 3. t-SNE plots of the degradation embeddings.

according to their properties. DSPFusion exhibits comparable performance to other methods on these metrics.

Qualitative results are presented in Fig. 2. When source images are affected by noise, denoising methods can remove noise but often at the cost of blurring fine details, such as texts on the wall and the license plate. By contrast, DSPFusion preserves rich texture while suppressing noise. In blurry scenarios, although HI-Diff partially mitigates the blur, DSPFusion delivers sharper visual clarity. This advantage arises from the fact that *our method can enhance the degraded modality by leveraging comprehensive semantic priors from both infrared and visible images, offering a more complete scene representation*. Conversely, single-modality enhancement methods rely solely on limited intra-modality information to infer degradation-free images, which naturally limits their enhancement performance. As shown in Fig. 2 (e) and (f), our method can effectively handle challenging scenarios where both in-



Figure 4. Visual comparison of object detection.

frared and visible images suffer from degradations. This is achieved by *employing modality-specific degradation priors in a divide-and-conquer manner to modulate the features of each modality individually, ensuring that the feature enhancement is precisely adapted to the unique characteristics of each modality*. Both quantitative and qualitative results demonstrate the superiority of DSPFusion in suppressing degradations and integrating complementary context across various degraded scenarios in a unified model.

4.3. Extended Experiments and Discussions

Degradation Prior Visualization. Figure 3 shows t-SNE visualizations illustrating the ability of various models to distinguish degradation types. While DA-CLIP can partially separate degradations in visible images, it performs poorly on infrared images. In contrast, our DPEN effectively distinguishes degradations across modalities, laying a solid foundation for subsequent restoration and fusion.

Table 3. Quantitative results of object detection.

Methods	Fusion in nighttime scenarios with enhancement					
	Prec.	Recall	AP@50	AP@75	AP@95	mAP
DeFus. [15]	0.983	0.831	0.911	0.802	0.057	0.684
PAIF [18]	0.989	0.848	0.919	0.799	0.071	0.683
MetaFus. [55]	0.958	0.871	0.927	0.806	0.116	0.697
LRRNet [13]	0.989	0.811	0.902	0.783	0.040	0.668
MURF [42]	0.980	0.884	0.935	0.809	0.095	0.707
SegMiF [17]	0.981	0.835	0.910	0.799	0.092	0.687
DDFM [57]	0.983	0.842	0.917	0.801	0.067	0.679
EMMA [58]	0.971	0.846	0.916	0.791	0.085	0.685
Text-IF [44]	0.989	0.782	0.887	0.778	0.043	0.667
DSPFusion	0.974	0.884	0.936	0.822	0.169	0.726

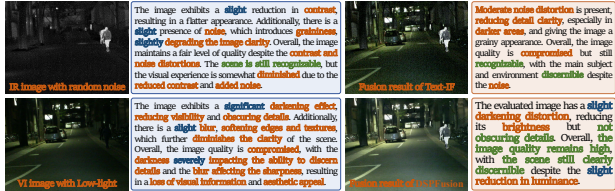


Figure 5. Evaluation results with DepictQA.

Object Detection. We also evaluate object detection performance on LLVIP to indirectly assess the fusion quality with re-trained YOLOv8 [27]. Qualitative and quantitative results are shown in Fig. 4 and Tab. 3. Owing to superior information restoration and integration, the detector identifies all pedestrians in our fusion results with higher confidence and achieves the best average precision (AP) across various confidence thresholds.

Evaluation with DepictQA. We introduce DepictQA [45], a descriptive image quality assessment metric based on vision language models, to evaluate our fused image quality. As shown in Fig. 5, the infrared image suffers from significant noise, while the visible image is affected by low-light. DepictQA not only accurately identifies these degradations but also describes their severity. Although Text-IF only mildly suppresses degradations, thanks to effective information aggregation, DepictQA judges that while its fusion result experiences moderate noise distortion, it remains recognizable. In contrast, DSPFusion successfully achieves low-light enhancement and noise reduction, along with effective information aggregation. Thus, DepictQA assesses our image quality as remaining high.

Computational Efficiency. We conduct the diffusion process in a compact space, greatly reducing computational costs. As shown in Tab. 4, compared to DDFM, which performs diffusion in the image space, DSPFusion exhibits a significant advantage, being over 29 faster than DDFM. Moreover, in comparison to Text-IF, which relies on an additional CLIP model for degradation prompting, DSPFusion also offers a notable improvement in efficiency. Specifically, in degraded scenarios, it offers a clear advantage by obviating the need for additional pre-processing.

Real-World Generalization. As shown in Fig. 6 (a)

Table 4. Computational efficiency comparison on MSRS dataset.

Methods	Fusion			Fusion with enhancement		
	parm.(m)	flops(g)	time(s)	parm.(m)	flops(g)	time(s)
DeFus. [15]	7.874	71.55	0.075	234.81	869.24	0.478
PAIF [18]	44.86	122.12	0.052	271.80	919.80	0.455
MetaFus. [55]	0.812	159.48	0.028	227.74	957.16	0.431
LRRNet [13]	0.049	14.17	0.085	226.98	811.86	0.488
MURF [42]	0.120	31.50	0.205	227.05	829.19	0.608
SegMiF [17]	45.04	353.7	0.147	271.97	1151.4	0.550
DDFM [57]	552.7	5220.	3.451	779.59	6018.2	3.861
EMMA [58]	1.516	41.54	0.037	228.45	839.23	0.440
Text-IF [44]	89.01	1518.9	0.157	89.01	1518.9	0.157
DSPFusion	13.99	254.34	0.119	13.99	254.34	0.119

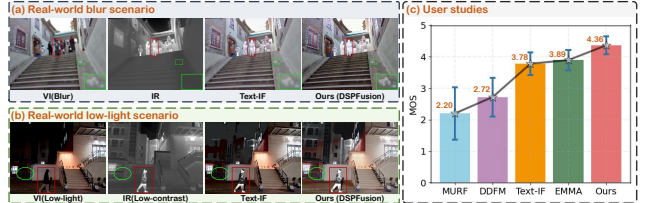


Figure 6. Generalization results in the real world and user studies.

Table 5. Quantitative results of the ablation studies.

Configs	Deg. prior	Sema. prior	VI(Blur)			VI(Rain)			IR(Stripe noise, SN)			VI(Rain) and IR(SN)						
			MUSIQ	PI	Tres	SF	MUSIQ	PI	Tres	SD	MUSIQ	PI	Tres	EN	MUSIQ	PI	Tres	
I	✓	✗	45.88	3.21	46.49	15.10	49.07	2.69	55.03	54.27	50.22	2.89	56.137	7.17	50.06	2.85	54.89	7.26
II	✓	✓	46.96	3.07	48.44	15.46	49.61	2.68	55.92	55.20	50.80	2.80	56.42	7.27	50.52	2.79	55.96	7.17
III	✓	✓	46.45	3.09	48.31	15.38	49.71	2.53	56.19	54.83	50.85	2.75	56.74	7.26	50.60	2.76	56.87	7.16
Ours	✓	✓	47.14	2.97	49.75	15.69	50.47	2.56	56.53	55.60	51.06	2.79	57.24	7.35	50.88	2.74	57.10	7.35

and (b), our method generalizes well to real-world scenarios. In the blur scenario, although the visible image suffers from blur degradation due to focal plane vibration, DSPFusion effectively restores textural details. Besides, in the low-light condition, our fusion result significantly enhances scene visibility while maintaining natural contrast.

User Studies. 30 participants are invited to score fusion results of 50 image pairs of various degradation settings or real-world scenarios. As shown in Fig. 6 (c), our method achieves the highest MOS, indicating that our results are more in line with user perception.

Ablation Studies. In order to demonstrate the effectiveness of our specific designs, we conduct ablation studies by individually removing either DPEN or SPEN in various degraded scenarios. From Tab. 5, one can find that both DPEN and SPEN play crucial roles in improving the performance of DSPFusion. Particularly, our method better reconciles degradation suppression with information aggregation by integrating degradation and semantic priors.

5. Conclusion

This work presents a degradation and semantic dual-prior guided framework for degraded image fusion. A degradation prior embedding network is designed to extract modality-specific degradation priors, guiding the unified model to purposefully address degradations. A semantic prior embedding network is developed to capture semantic prior from cascaded source images, enabling implicit com-

plementary information aggregation. Moreover, we devise a semantic prior diffusion model to restore high-quality scene priors in a compact space, providing global semantic guidance for subsequent restoration and fusion. Experiments on multiple degraded scenarios demonstrate our superiority in suppressing degradation and aggregating information.

References

- [1] Fanglin Bao, Xueji Wang, Shree Hari Sureshbabu, Gautam Sreekumar, Liping Yang, Vaneet Aggarwal, Vishnu N Boddeti, and Zubin Jacob. Heat-assisted detection and ranging. *Nature*, 619(7971):743–748, 2023. 1
- [2] Hanting Chen, Yunhe Wang, Tianyu Guo, Chang Xu, Yiping Deng, Zhenhua Liu, Siwei Ma, Chunjing Xu, Chao Xu, and Wen Gao. Pre-trained image processing transformer. In *Proceedings of the IEEE Conference on Computer Vision and Pattern Recognition*, pages 12299–12310, 2021. 2
- [3] Xiang Chen, Jinshan Pan, and Jiangxin Dong. Bidirectional multi-scale implicit neural representations for image deraining. In *Proceedings of the IEEE Conference on Computer Vision and Pattern Recognition*, pages 25627–25636, 2024. 6
- [4] Zheng Chen, Yulun Zhang, Ding Liu, Jinjin Gu, Linghe Kong, Xin Yuan, et al. Hierarchical integration diffusion model for realistic image deblurring. *Advances in Neural Information Processing Systems*, 36, 2024. 2, 3, 5, 6, 13, 16
- [5] Ziteng Cui, Kunchang Li, Lin Gu, Shenghan Su, Peng Gao, ZhengKai Jiang, Yu Qiao, and Tatsuya Harada. You only need 90k parameters to adapt light: a light weight transformer for image enhancement and exposure correction. In *Proceedings of the British Machine Vision Conference*, 2022. 6
- [6] Juntao Guan, Rui Lai, and Ai Xiong. Wavelet deep neural network for stripe noise removal. *IEEE Access*, 7:44544–44554, 2019. 6
- [7] Jonathan Ho, Ajay Jain, and Pieter Abbeel. Denoising diffusion probabilistic models. *Advances in Neural Information Processing Systems*, 33:6840–6851, 2020. 2, 5
- [8] Deepak Kumar Jain, Xudong Zhao, Germán González-Almagro, Chenquan Gan, and Ketan Kotecha. Multimodal pedestrian detection using metaheuristics with deep convolutional neural network in crowded scenes. *Information Fusion*, 95:401–414, 2023. 1
- [9] Xinyu Jia, Chuang Zhu, Minzhen Li, Wenqi Tang, and Wenli Zhou. Llvip: A visible-infrared paired dataset for low-light vision. In *Proceedings of the IEEE International Conference on Computer Vision*, pages 3496–3504, 2021. 6
- [10] Yitong Jiang, Zhaoyang Zhang, Tianfan Xue, and Jinwei Gu. Autodir: Automatic all-in-one image restoration with latent diffusion. In *Proceedings of the European Conference on Computer Vision*, 2024. 2
- [11] Boyun Li, Xiao Liu, Peng Hu, Zhongqin Wu, Jiancheng Lv, and Xi Peng. All-in-one image restoration for unknown corruption. In *Proceedings of the IEEE Conference on Computer Vision and Pattern Recognition*, pages 17452–17462, 2022. 2, 4, 13
- [12] Hui Li and Xiao-Jun Wu. Densefuse: A fusion approach to infrared and visible images. *IEEE Transactions on Image Processing*, 28(5):2614–2623, 2019. 1
- [13] Hui Li, Tianyang Xu, Xiao-Jun Wu, Jiwen Lu, and Josef Kittler. Lrrnet: A novel representation learning guided fusion network for infrared and visible images. *IEEE Transactions on Pattern Analysis and Machine Intelligence*, 45(9):11040–11052, 2023. 1, 2, 5, 6, 8, 13
- [14] Junyi Li, Zhilu Zhang, Xiaoyu Liu, Chaoyu Feng, Xiaotao Wang, Lei Lei, and Wangmeng Zuo. Spatially adaptive self-supervised learning for real-world image denoising. In *Proceedings of the IEEE Conference on Computer Vision and Pattern Recognition*, pages 9914–9924, 2023. 6
- [15] Pengwei Liang, Junjun Jiang, Xianming Liu, and Jiayi Ma. Fusion from decomposition: A self-supervised decomposition approach for image fusion. In *Proceedings of the European Conference on Computer Vision*, pages 719–735, 2022. 2, 5, 6, 8, 13
- [16] Jinyuan Liu, Xin Fan, Zhanbo Huang, Guanyao Wu, Risheng Liu, Wei Zhong, and Zhongxuan Luo. Target-aware dual adversarial learning and a multi-scenario multi-modality benchmark to fuse infrared and visible for object detection. In *Proceedings of the IEEE Conference on Computer Vision and Pattern Recognition*, pages 5802–5811, 2022. 1, 2
- [17] Jinyuan Liu, Zhu Liu, Guanyao Wu, Long Ma, Risheng Liu, Wei Zhong, Zhongxuan Luo, and Xin Fan. Multi-interactive feature learning and a full-time multi-modality benchmark for image fusion and segmentation. In *Proceedings of the IEEE International Conference on Computer Vision*, pages 8115–8124, 2023. 1, 5, 6, 8, 13
- [18] Zhu Liu, Jinyuan Liu, Benzhuang Zhang, Long Ma, Xin Fan, and Risheng Liu. Paif: Perception-aware infrared-visible image fusion for attack-tolerant semantic segmentation. In *Proceedings of the ACM International Conference on Multimedia*, pages 3706–3714, 2023. 1, 2, 5, 6, 8, 13
- [19] Ziwei Luo, Fredrik K. Gustafsson, Zheng Zhao, Jens Sjölund, and Thomas B. Schön. Controlling vision-language models for multi-task image restoration. In *International Conference on Learning Representations*, 2024. 2
- [20] Jiayi Ma, Wei Yu, Pengwei Liang, Chang Li, and Junjun Jiang. Fusiongan: A generative adversarial network for infrared and visible image fusion. *Information Fusion*, 48:11–26, 2019. 1, 2
- [21] Jiayi Ma, Linfeng Tang, Meilong Xu, Hao Zhang, and Guobao Xiao. Stdfusionnet: An infrared and visible image fusion network based on salient target detection. *IEEE Transactions on Instrumentation and Measurement*, 70: 5009513, 2021. 1
- [22] Jiayi Ma, Linfeng Tang, Fan Fan, Jun Huang, Xiaoguang Mei, and Yong Ma. Swinfusion: Cross-domain long-range learning for general image fusion via swin transformer. *IEEE/CAA Journal of Automatica Sinica*, 9(7):1200–1217, 2022. 1, 2, 4
- [23] Amanda C Muller and Sundaram Narayanan. Cognitively-engineered multisensor image fusion for military applications. *Information Fusion*, 10(2):137–149, 2009. 1
- [24] Ozan Özdenizci and Robert Legenstein. Restoring vision in adverse weather conditions with patch-based denoising dif-

- fusion models. *IEEE Transactions on Pattern Analysis and Machine Intelligence*, 45(8):10346–10357, 2023. 2
- [25] Vaishnav Potlapalli, Syed Waqas Zamir, Salman H Khan, and Fahad Shahbaz Khan. Promptir: Prompting for all-in-one image restoration. *Advances in Neural Information Processing Systems*, 36, 2024. 2
- [26] Alec Radford, Jong Wook Kim, Chris Hallacy, Aditya Ramesh, Gabriel Goh, Sandhini Agarwal, Girish Sastry, Amanda Askell, Pamela Mishkin, Jack Clark, et al. Learning transferable visual models from natural language supervision. In *Proceedings of the International Conference on Machine Learning*, pages 8748–8763, 2021. 2
- [27] Joseph Redmon, Santosh Divvala, Ross Girshick, and Ali Farhadi. You only look once: Unified, real-time object detection. In *Proceedings of the IEEE Conference on Computer Vision and Pattern Recognition*, pages 779–788, 2016. 8
- [28] Robin Rombach, Andreas Blattmann, Dominik Lorenz, Patrick Esser, and Björn Ommer. High-resolution image synthesis with latent diffusion models. In *Proceedings of the IEEE Conference on Computer Vision and Pattern Recognition*, pages 10684–10695, 2022. 2, 4, 5
- [29] Chitwan Saharia, Jonathan Ho, William Chan, Tim Salimans, David J Fleet, and Mohammad Norouzi. Image super-resolution via iterative refinement. *IEEE Transactions on Pattern Analysis and Machine Intelligence*, 45(4):4713–4726, 2023. 2
- [30] Yiming Sun, Bing Cao, Pengfei Zhu, and Qinghua Hu. Detection-driven infrared and visible image fusion network. In *Proceedings of the ACM International Conference on Multimedia*, pages 4003–4011, 2022. 2
- [31] Linfeng Tang, Yuxin Deng, Yong Ma, Jun Huang, and Jiayi Ma. Superfusion: A versatile image registration and fusion network with semantic awareness. *IEEE/CAA Journal of Automatica Sinica*, 9(12):2121–2137, 2022. 1
- [32] Linfeng Tang, Jiteng Yuan, and Jiayi Ma. Image fusion in the loop of high-level vision tasks: A semantic-aware real-time infrared and visible image fusion network. *Information Fusion*, 82:28–42, 2022. 1, 2
- [33] Linfeng Tang, Jiteng Yuan, Hao Zhang, Xingyu Jiang, and Jiayi Ma. Piafusion: A progressive infrared and visible image fusion network based on illumination aware. *Information Fusion*, 83:79–92, 2022. 1, 6
- [34] Linfeng Tang, Xinyu Xiang, Hao Zhang, Meiqi Gong, and Jiayi Ma. Divfusion: Darkness-free infrared and visible image fusion. *Information Fusion*, 91:477–493, 2023. 1, 2
- [35] Alexander Toet. The tno multiband image data collection. *Data in Brief*, 15:249–251, 2017. 6
- [36] Ashish Vaswani, Noam Shazeer, Niki Parmar, Jakob Uszkoreit, Llion Jones, Aidan N Gomez, Łukasz Kaiser, and Illia Polosukhin. Attention is all you need. *Advances in Neural Information Processing Systems*, 30, 2017. 2
- [37] Di Wang, Jinyuan Liu, Xin Fan, and Risheng Liu. Unsupervised misaligned infrared and visible image fusion via cross-modality image generation and registration. In *Proceedings of the International Joint Conference on Artificial Intelligence*, pages 3508–3515, 2022. 2
- [38] Wenjing Wang, Huan Yang, Jianlong Fu, and Jiaying Liu. Zero-reference low-light enhancement via physical quadruple priors. In *Proceedings of the IEEE Conference on Computer Vision and Pattern Recognition*, pages 26057–26066, 2024. 6, 13
- [39] Bin Xia, Yulun Zhang, Shiyin Wang, Yitong Wang, Xinglong Wu, Yapeng Tian, Wenming Yang, and Luc Van Gool. Diffir: Efficient diffusion model for image restoration. In *Proceedings of the IEEE Conference on Computer Vision and Pattern Recognition*, pages 13095–13105, 2023. 2, 3
- [40] Han Xu, Jiayi Ma, Junjun Jiang, Xiaojie Guo, and Haibin Ling. U2fusion: A unified unsupervised image fusion network. *IEEE Transactions on Pattern Analysis and Machine Intelligence*, 44(1):502–518, 2022. 6
- [41] Han Xu, Jiayi Ma, Jiteng Yuan, Zhuliang Le, and Wei Liu. Rfnnet: Unsupervised network for mutually reinforcing multi-modal image registration and fusion. In *Proceedings of the IEEE Conference on Computer Vision and Pattern Recognition*, pages 19679–19688, 2022. 2
- [42] Han Xu, Jiteng Yuan, and Jiayi Ma. Murf: Mutually reinforcing multi-modal image registration and fusion. *IEEE Transactions on Pattern Analysis and Machine Intelligence*, 45(10):12148–12166, 2023. 1, 2, 5, 6, 8, 13
- [43] Xunpeng Yi, Linfeng Tang, Hao Zhang, Han Xu, and Jiayi Ma. Diff-if: Multi-modality image fusion via diffusion model with fusion knowledge prior. *Information Fusion*, 110:102450, 2024. 1
- [44] Xunpeng Yi, Han Xu, Hao Zhang, Linfeng Tang, and Jiayi Ma. Text-if: Leveraging semantic text guidance for degradation-aware and interactive image fusion. In *Proceedings of the IEEE Conference on Computer Vision and Pattern Recognition*, pages 27026–27035, 2024. 1, 2, 4, 5, 6, 8, 13
- [45] Zhiyuan You, Zheyuan Li, Jinjin Gu, Zhenfei Yin, Tianfan Xue, and Chao Dong. Depicting beyond scores: Advancing image quality assessment through multi-modal language models. In *Proceedings of the European Conference on Computer Vision*, 2024. 8
- [46] Sihyun Yu, Kihyuk Sohn, Subin Kim, and Jinwoo Shin. Video probabilistic diffusion models in projected latent space. In *Proceedings of the IEEE Conference on Computer Vision and Pattern Recognition*, pages 18456–18466, 2023. 2
- [47] Jun Yue, Leyuan Fang, Shaobo Xia, Yue Deng, and Jiayi Ma. Dif-fusion: Towards high color fidelity in infrared and visible image fusion with diffusion models. *IEEE Transactions on Image Processing*, 32:5705–5720, 2023. 1, 2
- [48] Syed Waqas Zamir, Aditya Arora, Salman Khan, Munawar Hayat, Fahad Shahbaz Khan, and Ming-Hsuan Yang. Restormer: Efficient transformer for high-resolution image restoration. In *Proceedings of the IEEE Conference on Computer Vision and Pattern Recognition*, pages 5728–5739, 2022. 2, 3, 5
- [49] Hao Zhang, Han Xu, Xin Tian, Junjun Jiang, and Jiayi Ma. Image fusion meets deep learning: A survey and perspective. *Information Fusion*, 76:323–336, 2021. 1
- [50] Hao Zhang, Linfeng Tang, Xinyu Xiang, Xuhui Zuo, and Jiayi Ma. Dispel darkness for better fusion: A controllable visual enhancer based on cross-modal conditional adversarial

- learning. In *Proceedings of the IEEE Conference on Computer Vision and Pattern Recognition*, pages 26487–26496, 2024. [1](#)
- [51] Jing Zhang, Aiping Liu, Dan Wang, Yu Liu, Z Jane Wang, and Xun Chen. Transformer-based end-to-end anatomical and functional image fusion. *IEEE Transactions on Instrumentation and Measurement*, 71:5019711, 2022. [1](#)
- [52] Jiaming Zhang, Huayao Liu, Kailun Yang, Xinxin Hu, Ruiping Liu, and Rainer Stiefelhagen. Cmx: Cross-modal fusion for rgb-x semantic segmentation with transformers. *IEEE Transactions on Intelligent Transportation Systems*, 24(12):14679–14694, 2023. [1](#)
- [53] Xingchen Zhang and Yiannis Demiris. Visible and infrared image fusion using deep learning. *IEEE Transactions on Pattern Analysis and Machine Intelligence*, 45(8):10535–10554, 2023. [1](#)
- [54] Yue Zhang, Bin Song, Xiaojiang Du, and Mohsen Guizani. Vehicle tracking using surveillance with multimodal data fusion. *IEEE Transactions on Intelligent Transportation Systems*, 19(7):2353–2361, 2018. [1](#)
- [55] Wenda Zhao, Shigeng Xie, Fan Zhao, You He, and Huchuan Lu. Metafusion: Infrared and visible image fusion via meta-feature embedding from object detection. In *Proceedings of the IEEE Conference on Computer Vision and Pattern Recognition*, pages 13955–13965, 2023. [1](#), [2](#), [5](#), [6](#), [8](#), [13](#)
- [56] Zixiang Zhao, Haowen Bai, Jianshe Zhang, Yulun Zhang, Shuang Xu, Zudi Lin, Radu Timofte, and Luc Van Gool. Cddfuse: Correlation-driven dual-branch feature decomposition for multi-modality image fusion. In *Proceedings of the IEEE Conference on Computer Vision and Pattern Recognition*, pages 5906–5916, 2023. [2](#)
- [57] Zixiang Zhao, Haowen Bai, Yuanzhi Zhu, Jianshe Zhang, Shuang Xu, Yulun Zhang, Kai Zhang, Deyu Meng, Radu Timofte, and Luc Van Gool. Ddfm: Denoising diffusion model for multi-modality image fusion. In *Proceedings of the IEEE International Conference on Computer Vision*, pages 8082–8093, 2023. [1](#), [2](#), [4](#), [5](#), [6](#), [8](#), [13](#)
- [58] Zixiang Zhao, Haowen Bai, Jianshe Zhang, Yulun Zhang, Kai Zhang, Shuang Xu, Dongdong Chen, Radu Timofte, and Luc Van Gool. Equivariant multi-modality image fusion. In *Proceedings of the IEEE Conference on Computer Vision and Pattern Recognition*, pages 25912–25921, 2024. [5](#), [6](#), [8](#), [13](#)

DSPFusion: Image Fusion via Degradation and Semantic Dual-Prior Guidance

Supplementary Material

A. More Details About Methodology Designs

In this section, we provide more details about our methodology designs. Figure 7 presents the network architecture of our prior-guided fusion module (PGFM). Given the global semantic prior p_s , which integrates high-quality and comprehensive scene contexts, we utilize a semantic channel attention, consisting of two linear layers, to generate a channel-wise fusion weight (w_{ir}^c or w_{vi}^c). Additionally, a spatial attention is employed to achieve spatial activity level measurements. The infrared (or visible) features are compressed along the channel dimension via global max pooling (GMP) and global average pooling (GAP). The pooled results are then concatenated along the channel dimension and fed into a convolutional layer to generate spatial weights (w_{ir}^s or w_{vi}^s). Subsequently, we comprehensively integrate the channel- and spatial-wise attention to obtain the final fusion weight, formulated as:

$$w_{ir} = \sigma(w_{ir}^c \otimes w_{ir}^s), \quad w_{vi} = \sigma(w_{vi}^c \otimes w_{vi}^s), \quad (16)$$

where \otimes denotes element-wise multiplication with broadcasting, and σ is the sigmoid function. Finally, the fusion process is defined as:

$$\mathcal{F}_f = w_{ir}\mathcal{F}_{ir} \oplus w_{vi}\mathcal{F}_{vi}. \quad (17)$$

Additionally, unlike the encoder layer, the prior-modulated decoder layer employs the semantic prior integration module instead of the dual-prior guidance module, relying solely on high-quality scene semantic priors to support feature reinforcement. This design aims to effectively eliminate the influence of degradation factors during the feature encoding stage with the assistance of degradation and semantic priors. After feature fusion, if fused features still contain mixed degradations, their distribution will differ from that of a single degradation, making it challenging for the degradation prior to characterize them accurately.

Figure 8 presents the schematic diagram of our contrastive mechanism for constraining the degradation prior embedding network. This section focuses on the criteria for selecting the positive and negative samples. The number of positive samples, K , is set to 3, and the number of negative samples, M , is set to 7. For instance, the degradation types of the anchors in visible and infrared images are low-light and low-contrast, respectively. For visible images, the positive samples consist of 3 low-light visible images from different scenes, while for infrared images, the positive samples are 3 low-contrast infrared images from different scenes. We then select 6 negative samples for

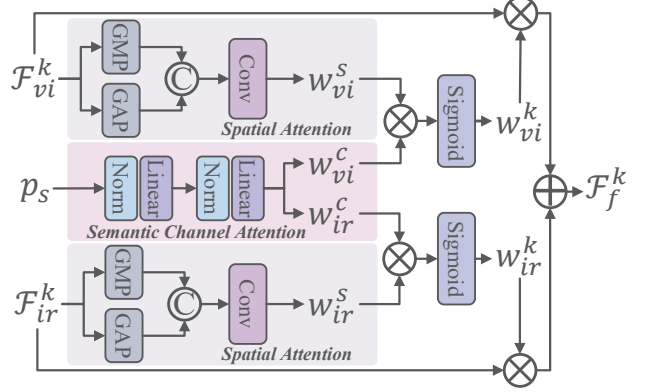


Figure 7. The architecture of the PGFM.

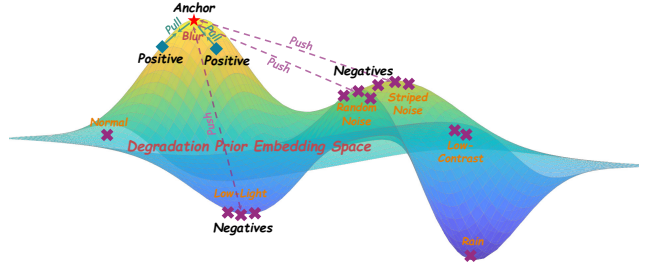


Figure 8. Schematic diagram of the contrastive mechanism.

both visible and infrared anchors from the remaining visible or infrared images with the same scene content as the anchors, where the visible images suffer from over-exposure, blur, rain, random noise, or no degradation, while the infrared images are affected by random noise, stripe noise, or no degradation. Moreover, the infrared anchor is added as the negative sample for the visible anchor, and vice versa. Therefore, for each anchor, there are 3 positive samples and 7 negative samples.

B. More Experiment Details

B.1. Implementation Details

We construct the training data on the EMS dataset¹, where the degradation types for visible images include blur, rain, low-light, over-exposure, and random noise, and the degradations for infrared images include low-contrast, random noise, and stripe noise. In particular, VI(Blur) uses Gaussian blur (kernel size = 21, $\sigma = 2.6$) to attenuate high-frequency details. VI(Rain) simulates rain stripes. VI(RN) and IR(RN) are influenced by Gaussian noise ($\mu = 0$,

¹<https://github.com/XunpengYi/EMS>

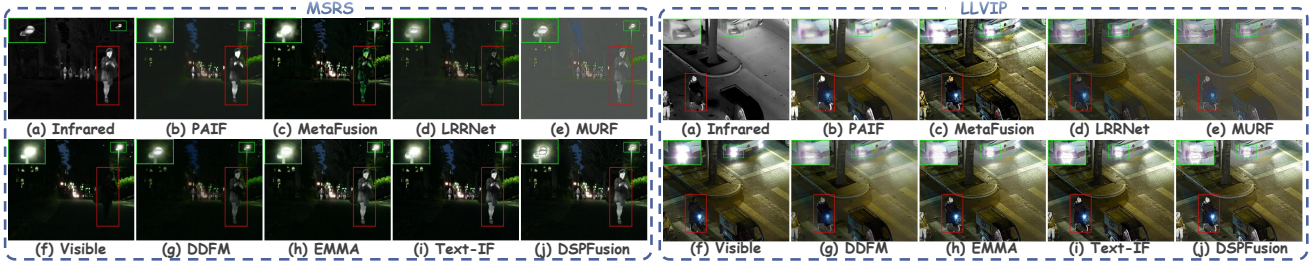


Figure 9. Visualization of fusion results on the typical fusion datasets.



Figure 10. Visualization of fusion results in degradation scenarios with pre-enhancement.

$\sigma = 10$) and Poisson noise ($\mu \in [70, 90]$). IR(SN) combines Gaussian noise ($\mu = 0, \sigma \in [10, 15]$) and stripe noise ($\mu \in [20, 30]$). We further extend this dataset by introducing low-light scenes from the MSRS dataset, where the visible images are enhanced by QuadPrior [38]. Therefore, VI(LL) from MSRS and LLVIP, VI(OE) from RoadScene, and IR(LC) from MSRS. Finally, our training dataset consists of 2,210 paired high-quality infrared and visible images. The source infrared images include 2,210 degradation-free images, 2,210 low-contrast images, 2,210 images with random noise, and 2,210 images with stripe noise. The source visible images involve 2,210 degradation-free images, 2,210 blurred images, 2,210 rain-affected images, 2,210 images with random noise, 1,316 low-light images, and 136 over-exposed images. The contrastive learning configuration follows AirNet [11] and sampling steps refer to Hi-Diff [4]. All experiments are conducted on the NVIDIA RTX 4090 GPUs and 2.50 GHz Intel(R) Xeon(R) Platinum 8180 CPUs with PyTorch.

B.2. Experiment Configures

The nine state-of-the-art fusion methods includes DeFusion [15], PAIF [18], MetaFusion [55], LRRNet [13], MURF [42], SegMiF [17], DDFM [57], EMMA [58], Text-

IF [44]. The numbers of test images in the MSRS, LLVIP, RoadScene, and TNO datasets are 361, 50, 50, and 25, respectively, for quantitative fusion comparison without enhancement. When quantitatively evaluating performance under degradation scenarios, all scenarios include 100 test samples, except for the over-exposed scenario in visible images, which contains 50 test samples. For a fair comparison, almost all fusion algorithms apply state-of-the-art image restoration methods to pre-enhance source images. Notably, Text-IF [44] utilizes its built-in enhancement module for low-light and over-exposed visible images, as well as low-contrast and random noise in infrared images, while applying pre-processing algorithms for other degradation scenarios. Additionally, when source images are affected by random noise, PAIF [18] does not employ additional denoising algorithms for pre-enhancement, as its fusion network is inherently robust to noise.

C. More Results and Analysis

Figure 9 presents representative visual fusion results on the MSRS and LLVIP datasets. We can find that MetaFusion, LRRNet, MURF, and DDFM diminish the prominence of thermal targets, while PAIF, EMMA, and Text-IF struggle to outline streetlights and headlights in overexposed con-

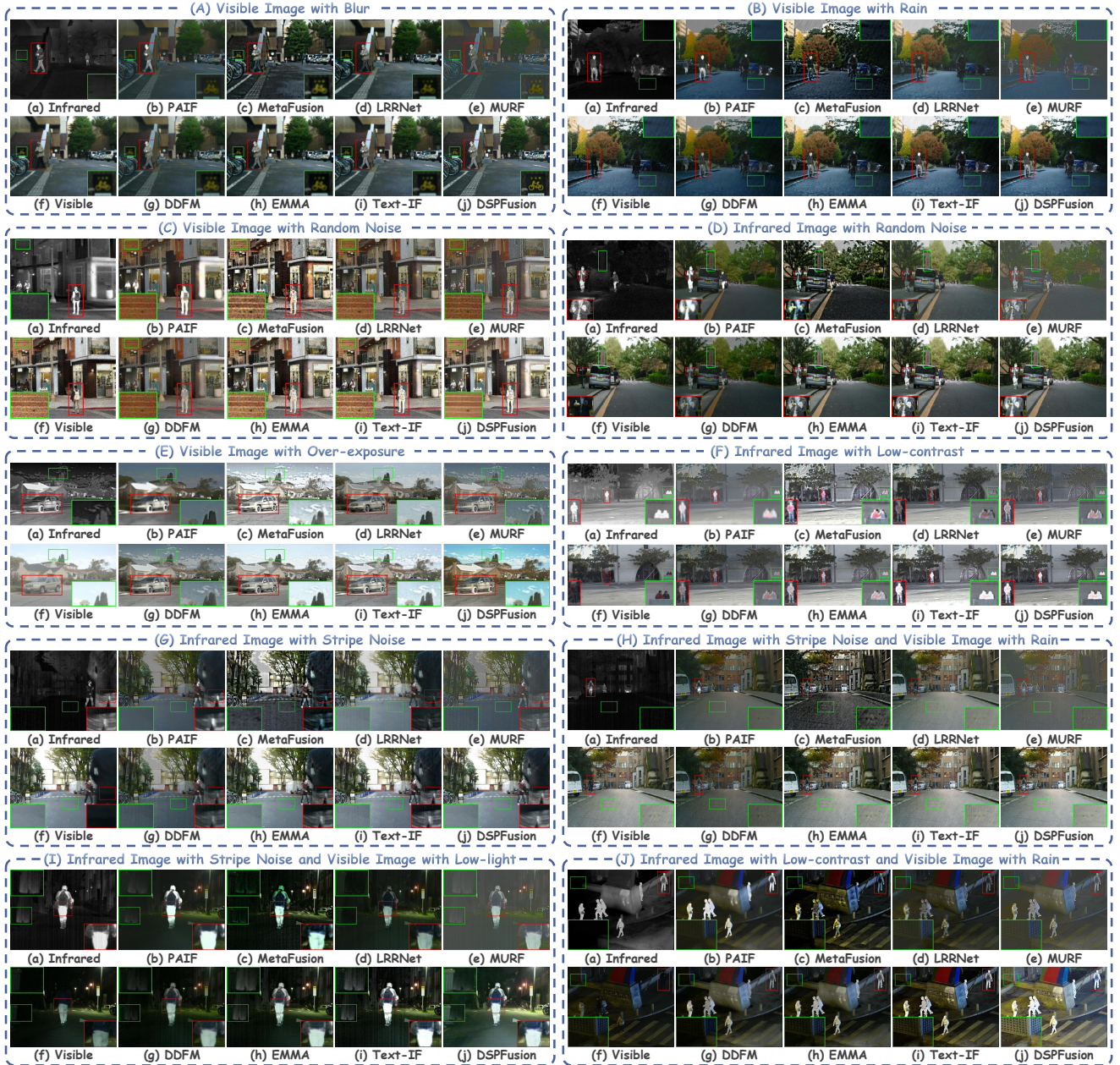


Figure 11. Visualization of fusion results in degradation scenarios without pre-enhancement.

ditions. In contrast, DSPFusion simultaneously highlights significant targets and preserves abundant textures. Overall, the quantitative and qualitative results collectively demonstrate the impressive fusion performance of our DSPFusion.

In the degradation scenarios, besides using no-reference image quality assessment metrics, *i.e.*, MUSIQ, PI, and TRaS, we also utilize statistical metrics frequently employed in the image fusion field to assess performance based on the properties of degradations. In detail, when source images are affected by blurring, textures become obscured.

Therefore, we use the SF metric to evaluate the richness of details in the fusion results. Additionally, when source images suffer from issues such as low light, overexposure, or low contrast, the overall contrast diminishes. Consequently, we use the SD metric to assess the effectiveness of the fusion results in counteracting these degradations. Furthermore, when images are affected by noise or rain, both SF and SD values may be artificially inflated, so we employ the EN metric to evaluate the fusion performance accurately.

Figure 10 provides more fusion results in the degrada-

Table 6. Computational efficiency of pre-enhancement algorithms.

Task	Deblurring	Deraining	Denoising	Low-light enhancement	Exposure correction	Stripe noise remove	Average
Method	Hi-Diff	NeRD-Rain	Spadap	QuadPrior	IAT	WDNN	
Parm. (M)	24.152	22.856	1.084	1313.39	0.087	0.013	226.93
Flops (G)	529.359	693.649	81.875	3473.413	6.728	1.105	797.688
Time (s)	0.359	0.299	0.003	1.745	0.007	0.003	0.403

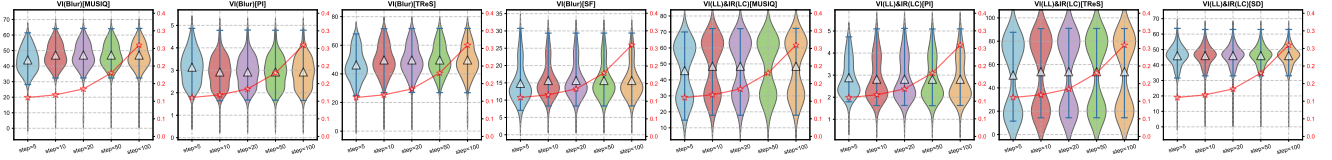


Figure 12. Quantitative analysis of various sampling steps.

tion scenarios with enhancement. From Fig 10, one can find that PAIF obscures texture details within the scenes, particularly in prominent infrared targets, despite the excessive enhancement of these targets. This is attributed to PAIF attempting to counteract noise. Additionally, MetaFusion introduces artificial textures during the fusion process, which is the primary factor for its higher SF metric. We believe this is caused by MetaFusion paying more attention to the object detection task, resulting in insufficient consideration for visual perception. LRRNet, MURF, and DDFM seem to simply neutralize infrared and visible images, resulting in their fusion results that reduce the prominence of infrared targets and cause a loss of texture details in the visible images. EMMA relies on manually selected fused images from existing fusion algorithms for supervision, which limits its performance potential. For instance, while EMMA can aggregate complementary information from source images across most scenarios, it may slightly diminish the prominence of infrared targets. Although Text-IF demonstrates good fusion performance, it still has several notable shortcomings. Firstly, Text-IF is highly sensitive to text prompts. As shown in our main manuscript, when we prompt it that the visible and infrared images suffer from degradations (such as low light and low contrast) simultaneously, it fails to mitigate the effects of degradations, even though it handles individual degradations effectively, as demonstrated in Fig. 10 (C) and (D). This may be caused by the fact that the feature embedding of such coupled text prompts is unfamiliar to the pre-trained model. Additionally, it is limited to addressing only a few specific types of degradations, such as low-light and over-exposure in visible images as well as random noise and low-contrast in infrared images. In contrast, our method adaptively iden-

tifies degradation types from the source images, enabling it to effectively handle the common degradations and achieve complementary information aggregation. Moreover, by employing a divide-and-conquer manner to address degradations in infrared and visible images separately, it remains effective even when both infrared and visible images suffer from degradations simultaneously.

Figure 11 presents the qualitative comparison results in degradation scenarios without pre-enhancement. It is evident that although most fusion algorithms can effectively aggregate complementary information, they are hindered by degradations and cannot provide satisfactory fusion outcomes. PAIF is capable of handling noise-related degradations, but it tends to blur the structures and details in the scene, resulting in suboptimal results. Text-IF can address illumination degradation in visible images, as well as low contrast and random noise in infrared images, but it is ineffective against other common degradations. In contrast, our DSPFusion is able to consistently synthesize impressive fusion results across all degradation conditions. This is attributed to the fact that our degradation prior embedding network can adaptively identify degradation types, and semantic prior diffusion model effectively recovers high-quality semantic priors. The degradation priors and high-quality semantic priors complement each other, jointly guiding the restoration and fusion model.

Effects of Sampling Steps. The impact of different sampling steps on fusion performance is illustrated in Fig. 12. The results reveal a nearly linear relationship between inference time and the number of sampling steps. Notably, when the number of sampling steps exceeds 10, further increases do not lead to a significant improvement in fusion performance. Consequently, we set the number of sampling steps

to 10 to strike a balance between fusion quality and sampling time, which is also the default setting in Hi-Diff [4].

Computational Efficiency of Pre-enhancement. Table 6 illustrates the computational efficiency of different pre-enhancement algorithms. From the results, we can find that some pre-enhancement algorithms, such as Spadap, IAT, and WDNN, are computationally efficient, while others, like Hi-Diff, NeRD-Rain, and QuadPrior, introduce heavy computational burdens. In particular, QuadPrior incurs significant computational costs as it conducts the diffusion process in the image domain. Our semantic prior diffusion model recovers high-quality semantic priors in a compact latent space, which greatly conserves computational overhead. We employ task-specific SOTA image enhancement methods for pre-enhancement, rather than relying on general approaches. On the one hand, general methods cannot simultaneously handle degradations in both infrared and visible modalities. On the other hand, general methods exhibit poor generalization on the infrared and visible image fusion datasets.